The Spectrum of the Damped Wave Operator for a Bounded Domain in R^2

Mark Asch and Gilles Lebeau

CONTENTS

The spectrum of the damped wave operator for a bounded domain in R^2 is shown to be related to the asymptotic average of the damping function by the geodesic flow. This allows the calculation of an asymptotic expression for the distribution of the imaginary parts of the eigenvalues for a radially symmetric geometry. Numerical simulations confirm the theoretical model. In addition, we are able to exhibit the beautiful structure of the spectrum and the close links between the eigenfunctions, the rays of geometrical optics, and the geometry of the damping region. The MATLAB code used in this paper is provided.

1. INTRODUCTION

1.1 The Problem

We consider the damped wave equation,

$$\begin{aligned} u_{tt} - c^2 \triangle u + 2a(x)u_t = 0 \quad &\text{in} \quad Q = \Omega \times (0,T)\,, \quad (1\text{–}1)\\ u = 0 \quad &\text{on} \quad \Gamma \times (0,T)\,,\\ u(x,0) = u^0(x), \qquad u_t(x,0) = u^1(x) \quad &\text{in} \quad \Omega, \end{aligned}$$

where $a(x) \in L^\infty(\Omega)$ is a non-negative potential with support in $\omega \subset \Omega$ and $(u^0, u^1) \in X = H_0^1(\Omega) \times L^2(\Omega)$. If we choose as the unknown the vector,

$$\mathbf{U} = \begin{bmatrix} u \\ u_t \end{bmatrix},$$

we can rewrite (1–1) in the form

$$\begin{aligned} \mathbf{U}_t + A\mathbf{U} = \mathbf{0} \quad &\text{in} \quad Q = \Omega \times (0,T)\,, \qquad (1\text{–}2)\\ \mathbf{U}(x,0) = \mathbf{U}^0(x) \quad &\text{in} \quad \Omega, \end{aligned}$$

where $A : D(A) \longrightarrow X$ is the operator defined by

$$A = \begin{pmatrix} 0 & -Id \\ -c^2\triangle & 2a(x) \end{pmatrix}.$$

We want to examine the *distribution* of the eigenvalues of this operator, in the strip where they are localised, as

2000 AMS Subject Classification: Primary 35P20; Secondary 35B37, 49J20, 49K20, 93C20

Keywords: Spectrum, non-self-adjoint operator, damped wave equation

1058-6458/2003 $0.50 per page
Experimental Mathematics **12**:2, page 227

a function of the *geometry* of the support of the potential $a(x)$.

The eigenvalue problem for the non-self-adjoint, quadratic operator pencil generated by (1–1) is obtained by replacing u in (1–1) by

$$u(x,t) = e^{\lambda t}\phi(x).$$

We obtain from (1–2) the standard form

$$(\lambda\, Id + A)\Phi = 0, \qquad \Phi = \begin{bmatrix} \phi \\ \lambda\phi \end{bmatrix}.$$

The condition for the existence of nontrivial solutions is that $\lambda \in \Sigma(A)$ (the spectrum) or, in the finite dimensional case, that $\det(\lambda\, Id + A) = 0$. Since A has a compact inverse, its spectrum is discrete and symmetric with respect to the real axis. The strip of localisation of the eigenvalues is defined by $\xi^-(a) \le \mathrm{Re}(\lambda) \le \xi^+(a)$ where $\xi^-(a) = \inf\{\mathrm{Re}(\lambda) : \lambda \in \sigma(A)\}$ and $\xi^+(a) = \sup\{\mathrm{Re}(\lambda) : \lambda \in \sigma(A)\}$.

1.2 The Applications

There is considerable interest in this problem from the point of view of the applications. In all real control problems, the major problem facing engineers and physicists is the *placement* of sensors and actuators. It is well known that one should measure and act on regions which correspond to certain natural frequencies of the domain (bridge, airfoil, beam, ...). What was not known until now was the connection between the geometry of the control (damping) region and the modes. The theoretical and numerical results which follow shed some light on this connection and will hopefully provide useful tools for industrial applications.

Furthermore, the theoretical study of the spectrum of non-self-adjoint operators still lags behind that of self-adjoint operators. Our use of geometrical considerations has produced a debut of understanding of the structure of the spectrum. Indeed, in the case of the unit square (see below), we observe a beautiful structure of successive bifurcations (seen also by [Freitas 99]) and in the case of a disc, we obtain an expression for the asymptotic distribution of the eigenvalues.

1.3 Overview

Section 2 presents a theoretical study of the spectrum of the damped wave operator. Here, some known results are recalled and then a model is given which is the base for the asymptotic expression of Section 2.1 In Section 3, the numerical method used to study the problem is explained. Section 4 is a presentation of numerous numerical simulations which serve both to validate the results of Sections 2 and 2.1, and to investigate some quite realistic model geometries.

Previous work on the spectrum of the damped wave operator was concerned mainly with the determination of optimal decay rates and was performed mostly in the one-dimensional case (a vibrating string)—see [Cox and Zuazua 94] and [Freitas 98]. A more complicated one-dimensional problem, dealing with exact controllability was considered in [Shubov et al. 97]. A two-dimensional problem was treated in [Chen et al. 91], but their results were only valid for a one-dimensional wave equation. More recently, [Sjöstrand 00] has proved a result on the asymptotic distribution of the distribution of eigenvalues in the band of localisation. Our theoretical results (see Theorems 2.2 and 2.3) and examples can be considered as developments of the main theorem (Theorem 3) in [Sjöstrand 00].

2. SOME THEORY AND MODELS

In this section, we investigate some theoretical aspects of the spectrum of (1–1). To avoid the difficulties of the boundary value problem, we discuss the problem (1–1) on a Riemannian manifold (M, g) with a damped wave equation of the form

$$\begin{aligned} u_{tt} - P_2 u + 2a(x)u_t = 0 \qquad & (1\text{–}1') \\ u(x,0) = u^0(x) \quad , \quad u_t(x,0) = u^1(x)\ . & \end{aligned}$$

Here, P_2 is a self-adjoint differential operator of order two on M, of the form

$$P_2 = \triangle_g - 2P_1\,(x, D_x)\ ,$$

where $\triangle_g$ is the Laplace-Beltrami operator on M and $P_1\,(x, D_x)$ is a self-adjoint differential operator of order one on M. The function $a(x) \in C^\infty(M)$ takes real values.

The spectrum of (1–1′) is the set Σ of $\lambda \in \mathbb{C}$ such that the equation

$$\left(\lambda^2 - P_2 + 2\lambda a(x)\right)\, v = 0 \qquad (2\text{–}1)$$

admits a nontrivial solution. For $\lambda \in \Sigma$, the multiplicity of λ is the dimension of the generalised eigenspace of $(\lambda\, Id + A)$ with

$$A = \begin{pmatrix} 0 & -Id \\ -P_2 & 2a \end{pmatrix},$$

i.e., the rank of the spectral projector,

$$\frac{1}{2\pi i}\int_{|z-\lambda|=\varepsilon}(z\,Id+A)^{-1}\,dz\,.$$

For $\lambda=i\omega+\sigma\in\Sigma$ and $v\neq 0$ such that (2–1) holds true, we have

$$\mathrm{Im}\left\langle\left(\lambda^2-P_2+2\lambda a(x)\right)\,v|v\right\rangle_{L^2}=0,$$

which implies

$$2\omega\left[\int_M a|v|^2+\sigma\int_M|v|^2\right]=0\,.$$

Therefore, for $\omega\neq 0$, we get

$$\lambda=i\omega+\sigma\in\Sigma\ \text{ and }\ \omega\neq 0\Longrightarrow-\max(a)\leq\sigma\leq-\min(a)\,. \tag{2–2}$$

Clearly, one has $\lambda\in\Sigma\iff\bar\lambda\in\Sigma$ since $Q=\lambda^2-P_2+2\lambda a(x)$ is Fredholm with zero index and $Q^*=\bar\lambda^2-P_2+2\bar\lambda a(x)$. When $\lambda=\sigma\in\Sigma$ is real, we get

$$\sigma^2\int_M|v|^2+2\sigma\int_M a|v|^2+\int_M|dv|^2-\int\langle P_1v|v\rangle=0\,,$$

which implies that $|\sigma|$ is bounded and therefore, $\Sigma\cap\mathbb{R}$ is a finite set.

We are interested in the probability of the distribution of the damping σ of the spectrum in the high frequency limit. More precisely, for $R>0$, let μ_R be the probability on the real line defined by

$$\mu_R(I)=\frac{\#\left\{\lambda=i\omega+\sigma\in\Sigma\,,\,\sigma\in I\,,\ |\omega|\leq R\right\}}{\#\left\{\lambda=i\omega+\sigma\in\Sigma\,,\ |\omega|\leq R\right\}} \tag{2–3}$$

where the λ are repeated according to their multiplicities. The μ_R are a finite linear combination of Dirac measures and by (2–2) are supported in $[-\max(a)\,,-\min(a)\,]$. Our main interest is to understand the behaviour of μ_R for R large, and its relation with the average of the damping $a(x)$ on the geodesic flow.

Let

$$\mathbb{S}^*M=\{(x,\xi)\in T^*M,\,\|\xi\|_x=1\}$$

be the unit cotangent vector bundle on M, and let us denote by $\phi(t,\rho)\,,\ t\in\mathbb{R}\,,\ \rho\in\mathbb{S}^*M$ the geodesic flow on $\mathbb{S}^*M$. Let $\underline{a}(t,\rho)\,,\ t\in\mathbb{R}\,,\ \rho\in\mathbb{S}^*M$ be the average of $a(x)$ at time t by the geodesic flow

$$\underline{a}(t,\rho)=\frac{1}{t}\int_0^t a(x(\phi(s,\rho)))\,ds\,.$$

The Liouville measure $d\lambda$ on $\mathbb{S}^*M$ (normalized by $\lambda(\mathbb{S}^*M)=1$) is invariant by the geodesic flow ϕ, so by the Birkhoff Ergodic Theorem (see [Cornfeld 82]), the Borel subset of $\mathbb{S}^*M$,

$$E=\{\rho\,;\text{ the limits }\lim_{t\to\pm\infty}\underline{a}(t,\rho)\text{ exist and are equal}\},$$

is of full measure on $\mathbb{S}^*M$. (More precisely, one has $\nu(E)=1$ for any probability on $\mathbb{S}^*M$ invariant by the geodesic flow.)

We define the Birkhoff function $\mathrm{Bir}(\rho)$ on E by

$$\mathrm{Bir}(\rho)=\lim_{t\to\pm\infty}\underline{a}(t,\rho)\,.$$

We can therefore introduce a "geometric" damping probability associated to the damping function a,

$$\mu_{\mathrm{geom}}(I)=\int_{\mathrm{Bir}(\rho)\in-I}d\lambda\quad(I\text{ a Borel subset of }\mathbb{R}).$$

One may expect a close link between the asymptotic $(R\to\infty)$ of the probability of distribution of the eigenvalues and the Birkhoff function $\mathrm{Bir}(\rho)$. In this direction, the most optimistic result would be

> "There exists a unique weak limit μ_∞ of the family $\{\mu_R\}_{R\to\infty}$ and $\mu_\infty=\mu_{\mathrm{geom}}$" (2–4)

We shall see below that (2–4) is not true in general and we present some numerical experiments in the sequel.

To our knowledge, there exist two results which show a link between the measures μ_R and the asymptotic for t large of the average $\underline{a}(t,\rho)$. The first result is due to J. Sjöstrand [Sjöstrand 00]. Let us denote by b_+ (respectively, b_-) the essential supremum (respectively, minimum) of the Birkhoff function $\mathrm{Bir}(\rho)$ with respect to the Liouville measure on $\mathbb{S}^*M$. Then we have the following theorem.

Theorem 2.1. (Sjöstrand.) *The support of any weak limit of the sequence μ_R is contained in the interval $[-b_+\,,-b_-]$.*

Notice that if the geodesic flow is ergodic on $\mathbb{S}^*M$, we have $\mathrm{Bir}(\rho)=\fint_M a$ (Liouville almost everywhere), so by Sjöstrand's result, (2–4) is true in this case and more precisely

$$\underset{R\to\infty}{\text{w-}\lim}\mu_R=\delta_{[-\sigma=\fint_M a]},$$

so the spectrum accumulates on the average of the damping function $a(x)$. This result was first proved in the one-dimensional case by S. Cox and E. Zuazua [Cox and Zuazua 94].

The second result gives some information on the possible values of σ for which there exists a sequence $\lambda_n = i\omega_n + \sigma_n$ in the spectrum such that $\omega_n \to \infty$ and $\sigma_n \to \sigma$. Let $v_n \in L^2(M)$, normalized by $|v_n|_{L^2} = 1$, be a solution of

$$[\lambda_n^2 - P_2 + 2\lambda_n a(x)]\ v_n = 0\,. \tag{2–5}$$

Let $h = h_n = 1/\omega_n$. Multiplying (2–5) by h_n^2, one gets the semiclassical equation for v_n

$$\left[-(1+h^2P_2) + 2ih(a+\sigma_n) + h^2(\sigma_n^2 + 2a\sigma_n)\right]\ v_n = 0\,. \tag{2–6}$$

Let ν be any semiclassical measure on T^*M associated with the sequence $\{v_n\}$ (see P. Gerard [Gérard and Leichtman 93] for an exposition of semiclassical measures); the weak limit of $\{v_n\}$ is zero and up to extraction of a subsequence, ν is characterized by

$$\int_{T^*M} q(x,\xi)\,d\nu = \lim_{n\to\infty} \langle q(x,hD)v_n \,|\, v_n\rangle_{L^2(M)}\,,$$
$$q(x,\xi) \in C_0^\infty(T^*M)\,.$$

Then ν is a probability on T^*M and the assumptions $P_2 = \triangle_g + \text{order}(1)$ and (2–6) imply that the support of ν is contained in the unit cosphere bundle $\mathbb{S}^*(M)$. Moreover, (2–6) implies that ν satisfies the propagation equation

$$\int_{T^*M} \left[\{\xi^2 - 1, q\} + 4(a+\sigma)q\right]\ d\nu = 0\,.$$

In other words, ν is a probability on $\mathbb{S}^*M$ such that for any Borel subset A of $\mathbb{S}^*M$ and any t, one has

$$\nu(\phi_t(A)) = \int_A e^{2t[\sigma + \underline{a}(t,\rho)]}\,d\nu(\rho),$$

where $\phi_t(A) = \{\phi(t,\rho)\,;\,\rho \in A\}$. By Fatou's lemma, we get

$$\int_A \liminf_{t\to\pm\infty} e^{2t[\sigma+\underline{a}(t,\rho)]}\,d\nu(\rho) < +\infty,$$

which implies

$$\begin{aligned} \nu(\{\rho\,;\,\sigma + \liminf_{t\to+\infty} \underline{a}(t,\rho) \quad &> \quad 0\}) = 0\,, \\ \nu(\{\rho\,;\,\sigma + \limsup_{t\to-\infty} \underline{a}(t,\rho) \quad &< \quad 0\}) = 0\,. \end{aligned} \tag{2–7}$$

For $\rho \in \mathbb{S}^*M$, let $J_\rho \subset \mathbb{R}$ be the closed interval,

$$J_\rho = \begin{cases} [\liminf_{t\to+\infty} \underline{a}(t,\rho)\,,\ \limsup_{t\to-\infty} \underline{a}(t,\rho) < 0] \\ \qquad\qquad \text{if } \liminf_{t\to+\infty} \underline{a}(t,\rho) \le \limsup_{t\to-\infty} \underline{a}(t,\rho) \\ \emptyset \qquad\qquad \text{otherwise.} \end{cases}$$

One has $J_\rho = \{\text{Bir}(\rho)\}$ if $\rho \in E$ and from (2–7) we get the following theorem.

Theorem 2.2. *If $\lambda_n = i\omega_n + \sigma_n$ is a sequence in the spectrum such that $\lim \sigma_n = \sigma$, then*

$$\exists\ \rho \in \mathbb{S}^*M,\ \ -\sigma \in J_\rho\,. \tag{2–8}$$

Notice that if $\rho = (x,\xi)$ and $-\rho \overset{\text{def}}{=} (x,-\xi)$, then $\underline{a}(t,-\rho) = \underline{a}(-t,\rho)$ so if $J_\rho = \emptyset$, then $J_{-\rho} \neq \emptyset$.

We next turn to the study of the very special case where M is the sphere $\mathbb{S}^2 \subset \mathbb{R}^3$. In this case, the geodesic flow is periodic with period 2π and the quotient of $\mathbb{S}^*(\mathbb{S}^2)$ by the flow, the space θ of orbits, is the space of oriented great circles. Thus, θ is also a sphere $\mathbb{S}^2$. Here, the Birkhoff function is defined everywhere: It is the Radon transform of the damping a,

$$\text{Bir}(\rho) = \oint_{C_\rho} a\ ;\ \ C_\rho = \text{ great circle through } \rho.$$

One has $\text{Bir}(\rho) = \text{Bir}(-\rho)$ for any ρ. Theorem 2.3 can now be proved.

Theorem 2.3. *Let us assume that the coefficients of $P_1(x,D_x)$ and the function $a(x)$ are analytic on the sphere $\mathbb{S}^2$. Let $p_1(x,\xi)$ be the principal symbol of P_1 and $q(\rho) = \oint_{C_\rho} p_1(x,\xi)$, $\rho \in \theta$, be the average of p_1 on the orbit C_ρ.*

Let us assume that the following generic hypotheses on $\text{Bir}(\rho)$ and $q(\rho)$ hold true: $\text{Bir}(\theta) = [b_-\,,\,b_+]$ and $\text{Bir}^{-1}\{b_\pm\}$ is finite; $dq(\rho) \neq 0$ if $\rho \in \text{Bir}^{-1}\{b_-\} \cup \text{Bir}^{-1}\{b_+\}$.

Then there exists an $\varepsilon > 0$ such that the support of any weak limit of the sequence $\{\mu_R\}$ is contained in the interval $[-b_+ + \varepsilon\,,\,-b_- - \varepsilon]$.

Remark 2.4. This shows that (2–4) is not true in general and that the density of the spectrum may vanish in the neighbourhood of (-) the (essential) extrema of the Birkhoff function. This fact is by no means surprising: The Birkhoff function is defined as the average of $\text{Im}\,A = (A - A^*)/2i$, $A = \partial_t^2 - P_2 + 2a(x)\partial_t$ on the trajectories of $\text{Re}\,A = (A + A^*)/2$, so depends on the Hilbert structure of the space $\mathcal{H}$ on which A acts, while the spectrum defined by (2–1) is free of a deformation $\mathcal{H}_\sigma$ of $\mathcal{H}$, $\sigma \in [0,1]$, $\mathcal{H}_0 = \mathcal{H}$ if A acts on $\mathcal{H}_\sigma$ and any solution v of (2–1) belongs to $\cap\mathcal{H}_\sigma$. Of course, here it is the very special structure of the geodesic flow on $\mathbb{S}^2$ which allows the construction of such a deformation.

Proof: By the assumptions of analyticity of P_1 and a, there exists a fixed complex neighbourhood X of $\mathbb{S}^2$, such that any solution of (2–1) is the restriction to $\mathbb{S}^2$ of a holomorphic function on X. Let J be a zero-order complex

Fourier integral operator, close to the Id, such that

$$J \triangle J^{-1} = \triangle + R$$

where R is a zero-order pseudodifferential operator.

Let $\mathcal{X}$ be the complex canonical transformation associated with J; $\mathcal{X}$ is a holomorphic, homogeneous symplectomorphism of T^*X defined near $T^*\mathbb{S}^2 \setminus 0$. Let $\theta^{\mathbb{C}}$ be a complex neighbourhood of the orbit space θ. We have $\xi(\mathcal{X}(\rho))^2 = \xi(\rho)^2$, so $\mathcal{X}$ maps any subvariety $\{\xi^2 = \text{const.}\}$ of T^*X into itself and therefore induces a holomorphic map $f : \theta^{\mathbb{C}} \to \theta^{\mathbb{C}}$ defined near θ.

Let now $\lambda_n \in \Sigma$ and v_n such that (2–1) holds true. Let Q_0 and Q_1 be the analytic pseudodifferential operators on the sphere defined by $J\,a\,J^{-1} = Q_0$, $J\,P_2\,J^{-1} = \triangle - 2Q_1$. Let $u_n = J(v_n)$. Then $u_n \in L^2(\mathbb{S}^2)$ and satisfies

$$\left[\lambda_n^2 - (\triangle + R - 2Q_1) + 2\lambda_n Q_0\right]\ u_n = 0.$$

Let $q_0(x,\xi)$, $q_1(x,\xi)$ be the principal symbols of Q_0, Q_1, let $\alpha(x,\xi) = q_0(x,\xi) + \frac{1}{i} q_1(x,\xi)\big|_{|\xi|=1}$, and let $\underline{\alpha}(\rho) = \oint_{C_\rho} \alpha$ for $\rho \in \theta$. Then, if $\lambda_n = i\omega_n + \sigma_n$ and $\lim_{n\to\infty} \sigma_n = \sigma$, the above calculation (2–5 – 2–8) implies that

$$-\sigma \in (\mathrm{Re}\,\underline{\alpha})(\theta)\,.$$

By construction, we have

$$\underline{\alpha}(\mathcal{X}(\rho)) = \mathrm{Bir}(\rho) + \frac{q(\rho)}{i}\,.$$

If we choose $\mathcal{X}$ close to the Id, such that $\mathcal{X}^{-1} = Id + i\varepsilon\tau + O(\varepsilon^2)$ with $\tau : \mathbb{S}^2 \to \mathbb{R}^3$ such that $\tau(y)\cdot y \equiv 0$. Then we get

$$(\mathrm{Re}\,\underline{\alpha})(\rho) = \mathrm{Bir}(\rho) + \varepsilon\, dq(\rho)[\tau(\rho)] + O(\varepsilon^2)$$

so the result follows from the fact that we can choose τ such that $dq(\rho)[\tau(\rho)] < 0$ if $\rho \in \mathrm{Bir}^{-1}\{b_+\}$ and $dq(\rho)[\tau(\rho)] > 0$ if $\rho \in \mathrm{Bir}^{-1}\{b_-\}$. □

2.1 Asymptotic Distribution of the Eigenvalues

The most well-known asymptotic for the distribution of eigenvalues is Weyl's formula for the Laplacian operator. Let $N(t) = \sum_{\lambda_j \le t} \mathbf{1}$ be the number of eigenvalues less than t, then

$$N(t) \sim \frac{\mu_2(\Omega)}{4\pi}\, t\ , \quad \Omega \subset \mathbb{R}^2,$$
$$N(t) \sim \frac{\mu_3(\Omega)}{6\pi^2}\, t^{3/2}\ , \quad \Omega \subset \mathbb{R}^3$$

as $t \to \infty$ where $\mu_n(\Omega)$ is the area of Ω, a bounded open set in $\mathbb{R}^n$, $n = 1, 2$. Ideally, one would like to invert this formula in order to obtain an effective asymptotic expression for the j-th eigenvalue itself. However, even for a region where the eigenvalues are known explicitly (such as a square or a circle in $\mathbb{R}^2$), it is difficult to obtain such a formula directly [Kuttler and Sillito 84].

In the case of a disc with a rotationally invariant damping region, we find (by separation of variables and reduction to a one-dimensional semiclassical equation) the following expression for the asymptotic distribution:

$$P(\mathrm{Re}(\lambda) \in -I) = \frac{4}{\pi} \int_{m(t)\in I} \sqrt{1-t^2}\,dt \tag{2–9}$$

where

$$m(t) = \frac{1}{2\sqrt{1-t^2}} \int_t^1 \frac{r a(r)}{\sqrt{r^2 - t^2}}\,dr\,.$$

Indeed, in this case, the result (2–4) is true.

Example 2.5. If $a = a_0$ is constant, then $m = a_0/2$ and $a_0 \notin -I$ implies $P = 0$, whereas $a_0 \in -I$ implies $P = 1$.

Example 2.6. If

$$a = \begin{cases} 1 \text{ for } 0 \le r < r_0 \\ 0 \text{ for } r_0 \le r \le 1 \end{cases}$$

then

$$m(t) = \frac{\sqrt{r_0^2 - t^2}}{2\sqrt{1-t^2}}$$

for $t < r_0$ and $m(t) = 0$ for $t > r_0$. We thus obtain the following integral formula for the distribution function

$$P([-r,0]) = \frac{4}{\pi} \int_{r_0}^1 \sqrt{1-t^2}\,dt + \frac{16}{\pi} \int_{r_0}^1 \frac{(1-r_0)^{3/2}\ s}{\sqrt{r_0^2 - 4s^2}\,(4s^2-1)^2}\,ds\,, \quad r \le r_0/2\,. \tag{2–10}$$

3. THE DISCRETISATION OF THE EIGENVALUE PROBLEM

3.1 Formulation

The domain, Ω, is approximated by a net of equidistant, discrete points $\Omega_h = M_{ij}$ with $i, j = 1, 2, \ldots, N$ and $N = (1/h) + 1$. The Laplacian operator, $(\partial_{xx} + \partial_{yy})u$ is approximated in a standard way by a second order accurate, centred difference scheme,

$$\triangle_h u = \left(u_{i+1,j} + u_{i-1,j} + u_{i,j+1} + u_{i,j-1} - 4u_{i,j}\right)/h^2,$$

where $u_{i,j} = u(x_i, y_j)$. We thus obtain a nonsymmetric block matrix, $\mathbb{A}$, the discrete approximation of the operator A, of the form

$$\mathbb{A} = \begin{bmatrix} 0 & -Id \\ -c^2 \triangle_h & 2a_h \end{bmatrix}, \qquad (3\text{–}1)$$

where

$$Id = \begin{bmatrix} 1 & 0 & 0 & \dots & 0 \\ 0 & 1 & 0 & \dots & 0 \\ \dots & \dots & \dots & \dots & \dots \\ 0 & 0 & 0 & \dots & 1 \end{bmatrix}, \quad \triangle_h = \begin{bmatrix} -4 & 1 & 0 & \dots & 0 \\ 1 & -4 & 1 & \dots & 0 \\ \dots & \dots & \dots & \dots & \dots \\ 0 & 0 & \dots & 1 & -4 \end{bmatrix}$$

and a_h is a diagonal matrix with $a_{kk} = a(x_i, y_j)$. The value of k is determined by the numbering of the discrete points M_{ij}.

3.2 Numerical Method

We employ the most powerful numerical method available in order to compute the eigenvalues of the matrix $\mathbb{A}$: the *implicitly restarted Arnoldi-Lanczos method* of Sorenson [Sorenson 95]. This method is particularly well suited to large sparse matrices which in our computations can have dimensions of up to 10,000. This method is a generalisation of an inverse power method with subspace iteration. The restarting ensures the smallest possible memory requirements. In fact, one can approximate k eigenvalues in a space proportional to nk where n is the dimension of the matrix.

All of our computations were perfomed with MATLAB©. The code is freely available—see Section 5.

4. RESULTS OF THE NUMERICAL SIMULATIONS

Preliminary computations reveal that the distance of the strip from the imaginary axis is related to the diameter of ω. We also verified the Weyl asymptotic. Subsequently, we examined a number of geometrical configurations (see below): squares, discs, and a few realistic cases ("dog-bone," "football jersey"). In all the computations, we set $a(x) = 1$.

4.1 Unit Square with $a(x) = c$ on the Half Square

We compute the spectrum of the damped wave equation for $a(x) = c$ on half the unit square. The spectrum aligns itself along the vertical $\mathrm{Re}(\lambda) = -\frac{1}{2}\int a(x)dx$. In addition, we observe bifurcations on two branches (see Figure 1) corresponding to eigenvalues that are strongly or weakly damped. The successive bifurcations correspond to increasing frequencies of the eigenfunctions. This phenomenon has also been observed by P. Freitas [Freitas 99] and can be explained by means of a Fourier decomposition of the solution of (1–1).

We note that eigenfunctions corresponding to eigenvalues on the branch that is close to the imaginary axis (less damped) have their support in the part of the domain where $a(x) = 0$ (see Figure 2(a)), whereas eigenfunctions corresponding to eigenvalues on the branch that is furthest from the imaginary axis (more strongly damped) have their support in the part of the domain where $a(x) \neq 0$ (see Figure 2 (b)). We have effectively *separated* the spectrum of the non-self-adjoint operator A. The eigenfunctions corresponding to eigenvalues in the central trunk spread their energy over the entire domain as we can see in the Figure 2 (c). Note that there are two graphic representations for each eigenvector: a surface plot (upper part) and a contour plot (lower part).

The gap that can be seen in the central trunk of the eigenvalue plot (uppermost plot of Figure 1) is a consequence of the discretisation: Reducing the spatial discretisation from h to $h/2$ reduces the size of the gap by one half.

4.2 Damping on a Disc

In this section, we present graphic results for the spectrum over a disc. Three cases are treated (see Figure 3): damping in the interior, damping on an annulus, and damping on an offset disc. The first two cases satisfiy the hypotheses of the asymptotic formula (2–9) and comparisons can be made between the theoretical and numerical results.

4.2.1 Damping in an interior disc. In this case, we observe (as was the case for the square) the localisation of the strongly damped eigenfunctions in the region of damping. In addition, we reproduce numerically the asymptotic formula (2–10) for the distribution of the eigenvalues with $r_0 = 0.5$. We note that the asymptotic is attained relatively quickly. In Figures 4 and 5, we took $N = 64$, and computed the first 620 eigenvalues of the resulting matrix with $\mathrm{Im}(\lambda_{\max}) \approx 60$. We observe that the cumulative distribution function (antiderivative of the probability distribution) is of the right form. The probability distribution function itself is quite innacurate, but computations show that this can be improved by means of a finer discretisation. However, the computations then become extremely costly.

This comparison provides preliminary evidence in favor of the more general result (2–4) concerning the relation between the geometry and the spectrum.

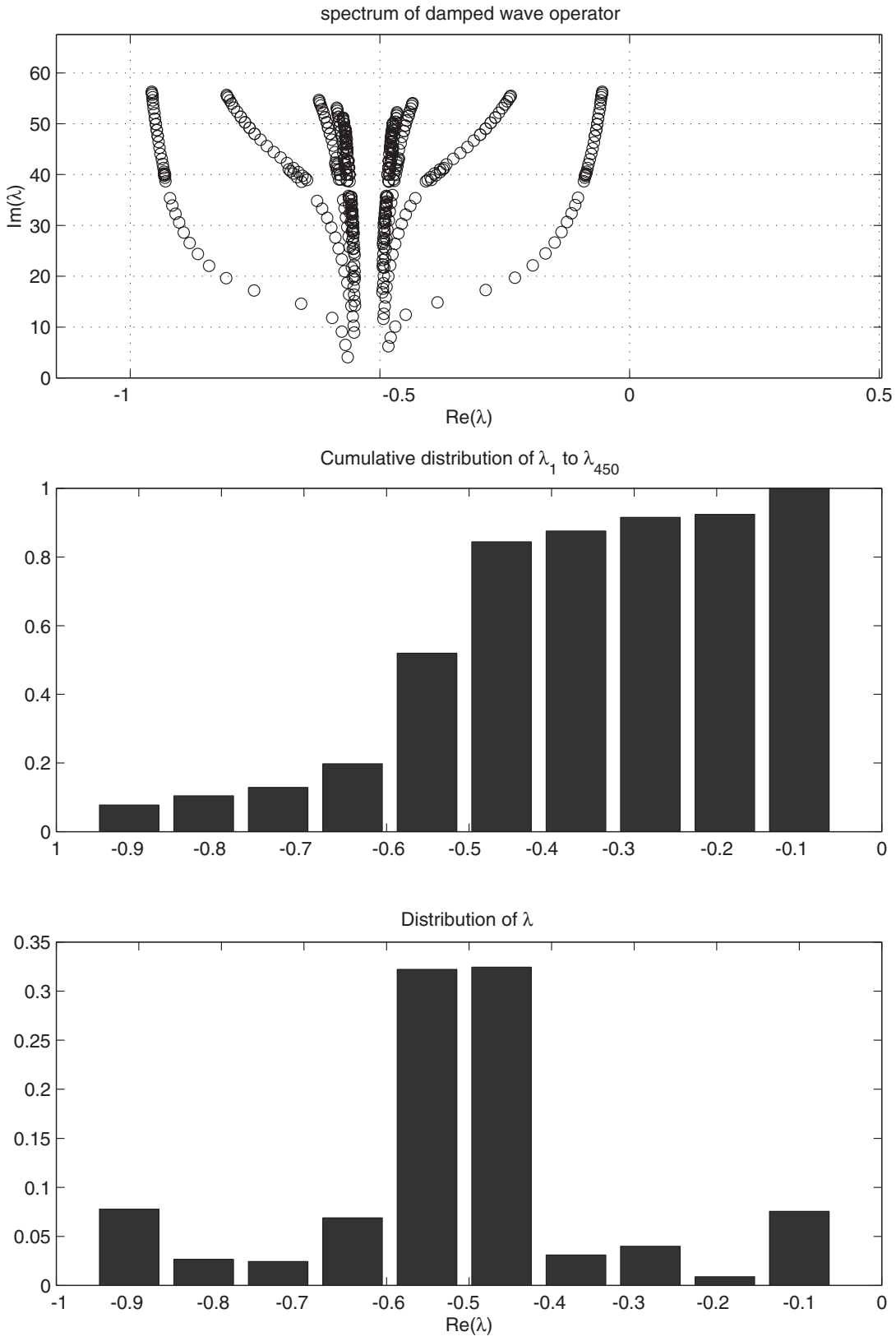

FIGURE 1. Distribution of eigenvalues for $a(x) = 1$ on the left half of the unit square.

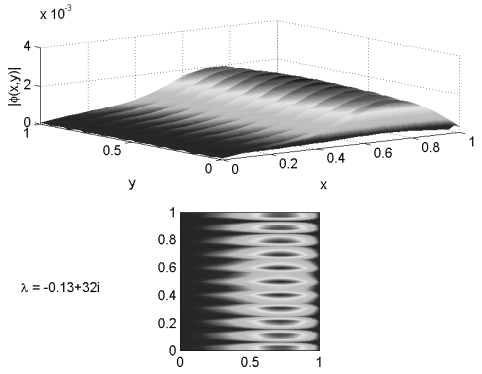

(a) Eigenfunction corresponding to lightly damped eigenvalue $\lambda = -0.13 + i\,32$.

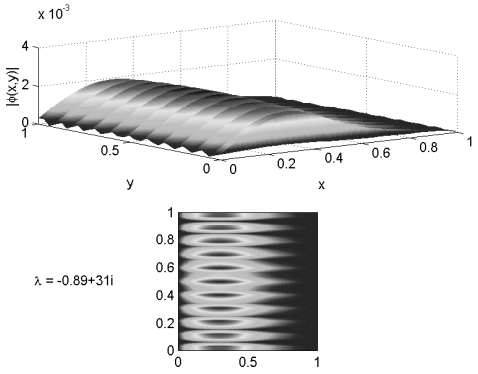

(b) Eigenfunction corresponding to strongly damped eigenvalue $\lambda = -0.89 + i\,31$.

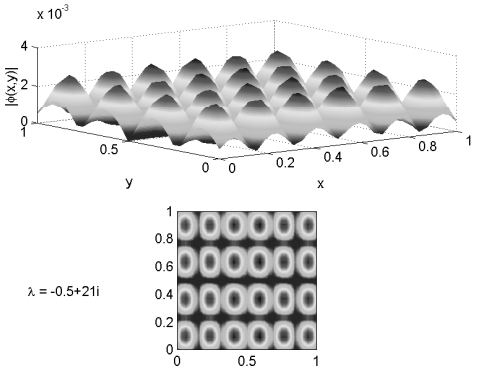

(c) Eigenfunction corresponding to an eigenvalue on the central trunk $\lambda = -0.5 + i\,21$.

FIGURE 2. Eigenfunctions for damping on the left half of the unit square.

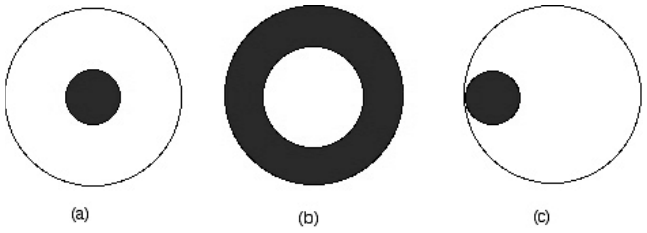

FIGURE 3. Damping geometries for the disc ($a(x) > 0$ in shaded region): (a) damping in an interior disc; (b) damping in exterior annulus; (c) damping in an offset disc.

4.2.2 Damping on an annulus. In this case, we again observe the phenomenon of localisation of the eigenfunctions correponding to strongly damped eigenvalues in the region where $a(x) > 0$. Damped eigenvalues correspond to whispering gallery modes whereas undamped modes are concentrated in the center of the disc. Numerical results are not shown here, but can be easily reproduced by the interested reader with the aid of the MATLAB code provided (see Section 5.). One could also verify the asymptotic formula (2–9).

4.2.3 Damping on an offset disc. When the damping is localised in an offset disc, we cannot expect the eigenfunctions corresponding to the strongly damped eigenvalues to be concentrated in the region of damping as in the other cases. This is due to the fact that rays cannot be trapped in such a region. However, we clearly observe the effect of the damping. The damped eigenfunctions are either whispering modes (see Figure 6(a)) or they are oriented towards the damping region as in Figure 6(c), whereas the undamped eigenfunctions are concentrated in the interior (see Figure 6(b)) or are oriented in such a way as to avoid the damping region as in Figure 6(d). This is precisely what one would expect from the point of view of the geometrical optics: Trajectories of undamped rays avoid the damping region. Once again, we seem to have a (qualitative) confirmation of the general result (2–4).

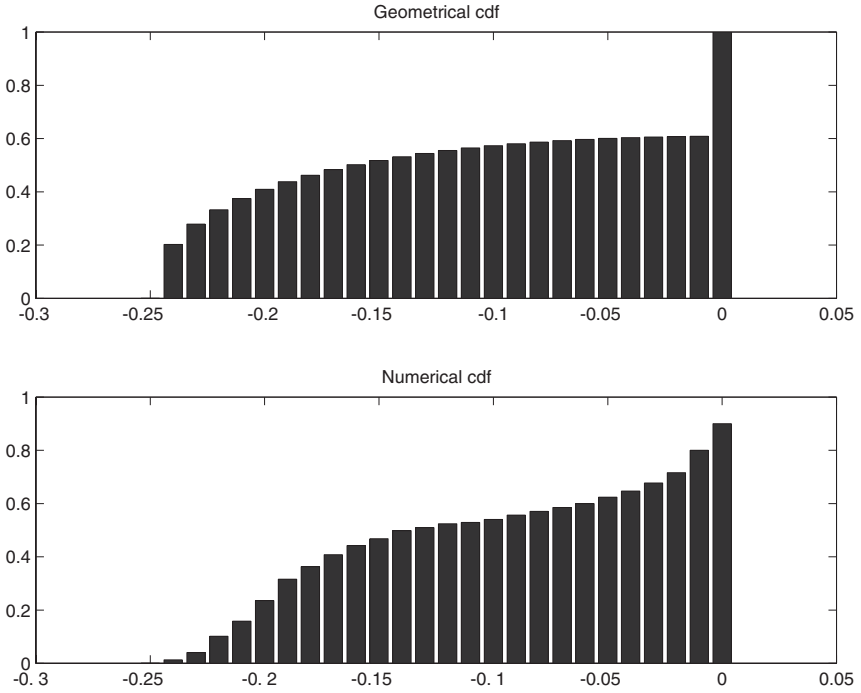

FIGURE 4. Cumulative distribution functions for damping in an interior disc of radius $r = 0.5$: comparison of the geometrical and numerical calculated distributions.

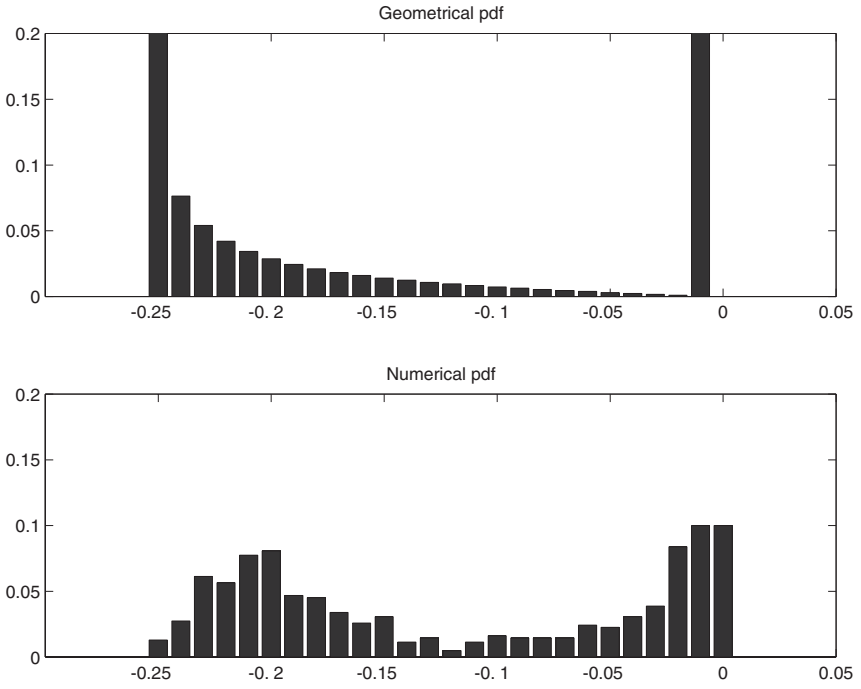

FIGURE 5. Probability distribution functions for damping in an interior disc of radius $r = 0.5$: comparison of the geometrical and numerically calculated distributions.

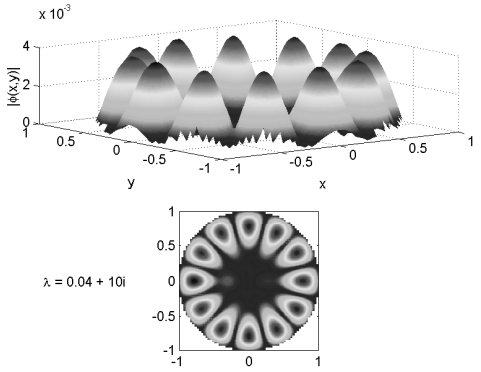

(a) Eigenfunction corresponding to strongly damped eigenvalue $\lambda = -0.04 + i\ 10$.

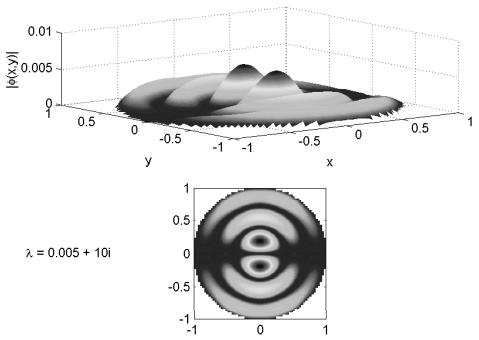

(b) Eigenfunction corresponding to lightly damped eigenvalue $\lambda = -0.005 + i\ 10$.

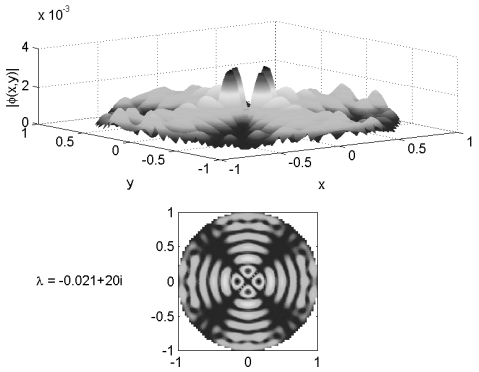

(c) Eigenfunction corresponding to strongly damped eigenvalue $\lambda = -0.021 + i\ 20$.

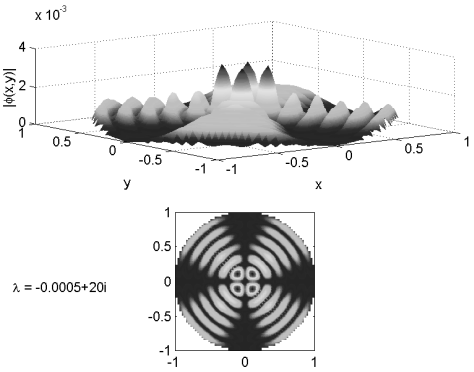

(d) Eigenfunction corresponding to lightly damped eigenvalue $\lambda = -0.0005 + i\ 20$.

FIGURE 6. Eigenfunctions for damping on an offset disc of radius $r = 0.2$ centred at $(-0.8, 0)$.

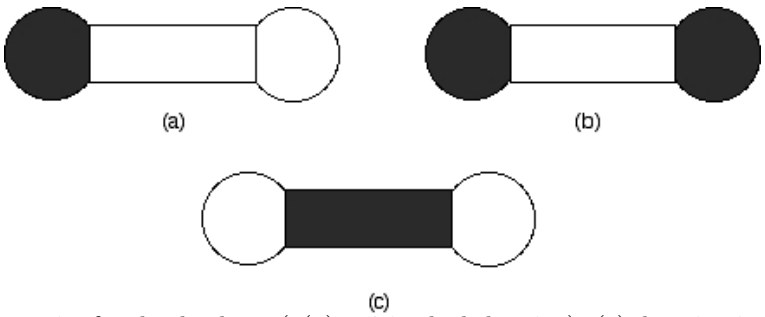

FIGURE 7. Damping geometries for the dog-bone ($a(x) > 0$ in shaded region): (a) damping in left disc; (b) damping in both discs; (c) damping in shaft.

4.3 Damping on a Dog Bone Shape

Here we take the famous dumbbell (or dog bone) shape. We consider several cases (see Figure 7) for the support of the damping function $a(x)$. This is an attempt to simulate "realistic" geometries.

First, we place the damping in the left-most disc (see Figure 8). The plots of the eigenfunctions are shown below in Figure 9 for different eigenvalues. We clearly observe that the eigenfunctions corresponding to strongly damped eigenvalues are concentrated in the left-

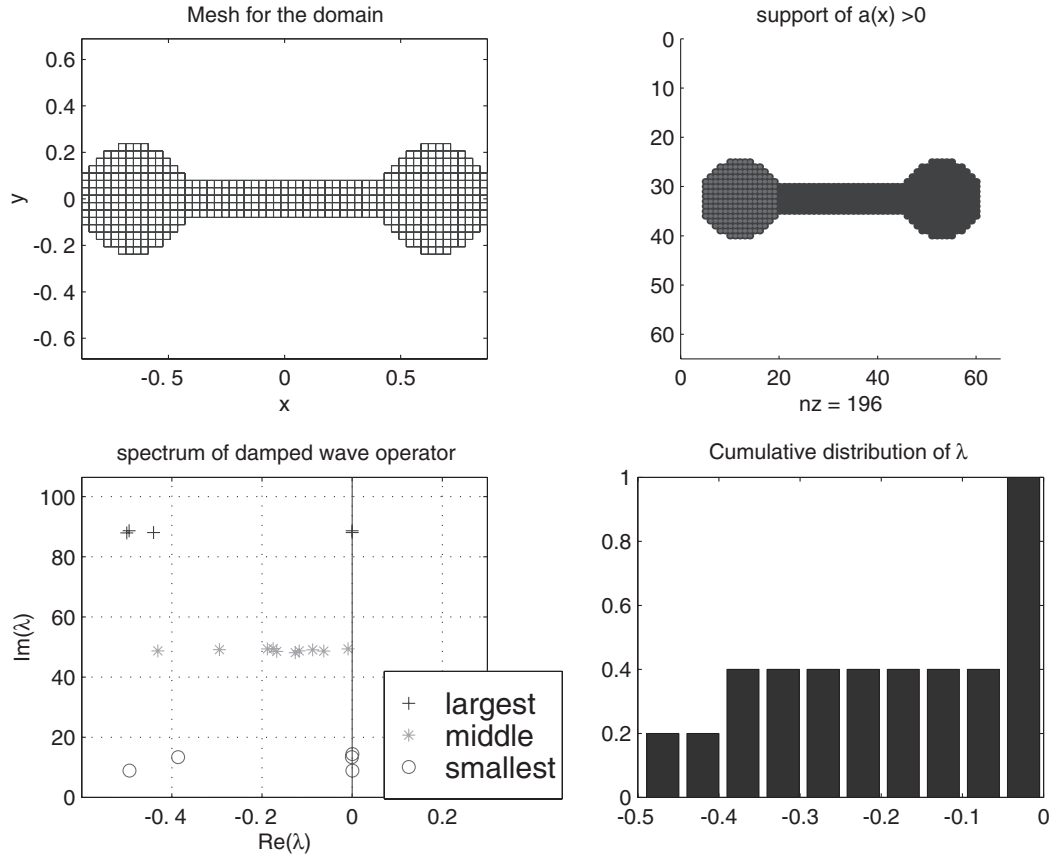

FIGURE 8. The dog-bone region with $a(x) = 1$ in the left-most disc: mesh, damping, eigenvalues.

most disc (see Figures 9(a), 9(c)), whereas the slightly damped ones concentrate in the shaft and the right-most disc as can be seen in Figures 9(b) and 9(d). The eigenfunction corresponding to an eigenvalue in the midrange, spreads its energy over the entire domain—see Figure 9(e).

When we damp in both extremities (see Figure 11), we observe the localisation of the eigenfunctions as expected; that is, localisation in the two discs of the strongly damped eigenfunctions (see Figures 10(a), 10(c)) and localisation in the shaft of the slightly damped ones (see Figure 10(b)). Averagely damped eigenfunctions spread their energy over the whole domain—see Figures 10(d) and 10(e). When the damping is concentrated in the shaft, we obtain the inverse effect.

4.4 Damping in the Sleeves of a Football Jersey

This geometry is composed of a half ellipse with two rectangles (the "sleeves") and a trapezoid (the bodice) placed below it (see Figure 13). The physical problem from which it is arises is the following: If one lights a candle (or makes a sound) in one of the sleeves, can it be seen (or heard) in the bodice area? From geometrical considerations, the half ellipse will reflect any rays emanating from the sleeves in such a way as to always avoid the bodice area. Thus, the answer to the above question is "no" (ignoring all diffraction effects).

Our numerical simulations reproduce this phenomenon. We place the damping in the two sleeves and plot the eigenvectors corresponding to strongly damped and to undamped eigenvalues. In Figure 12, we clearly see how the energy of the damped modes is concentrated on rays that do not reflect into the central area at all (Figure 12(a), 12(c)), whereas the energy of an undamped mode is confined to the half-ellipse and does not penetrate the sleeves (Figure 12(b)).

According to the geometrical optics, we would expect to find a gap in the spectrum between the modes confined to the sleeves and the modes confined in the half-ellipse. This is borne out by the simulations, where the eigenvalues are concentrated in two vertical strips (one close to the imaginary axis, one further to the left) and the few

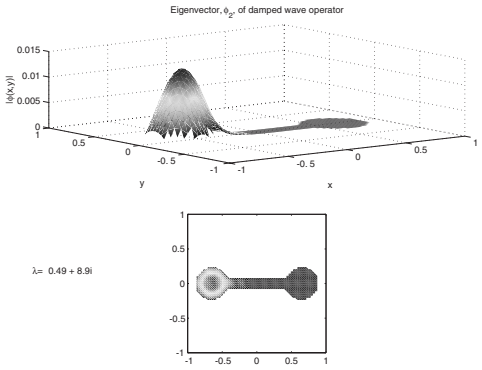

(a) Eigenfunction corresponding to strongly damped eigenvalue $\lambda = -0.49 + i\ 8.9$.

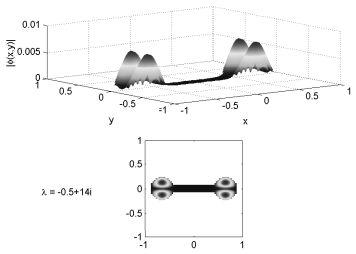

(b) Eigenfunction corresponding to lightly damped eigenvalue $\lambda = -4 \times 10^{-9} + i\ 8.9$.

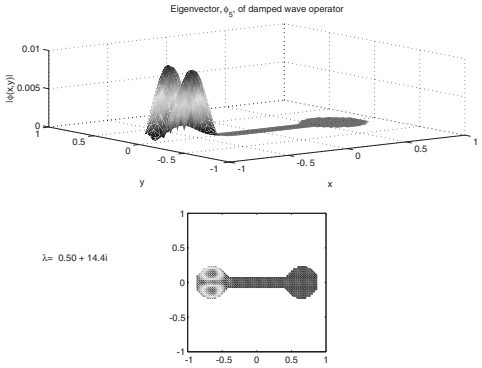

(c) Eigenfunction corresponding to strongly damped eigenvalue $\lambda = -0.5 + i\ 14.4$.

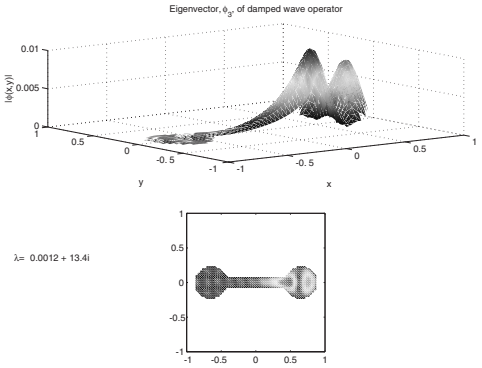

(d) Eigenfunction corresponding to lightly damped eigenvalue $\lambda = -0.0012 + i\ 13.4$

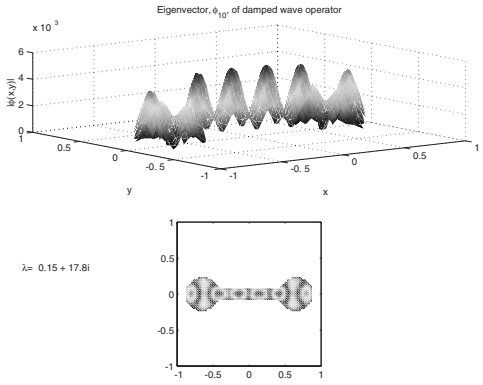

(e) Eigenfunction corresponding to an eigenvalue on the central trunk $\lambda = -0.15 + i\ 17.8$.

FIGURE 9. Eigenfunctions for damping on the left disc of the dog-bone.

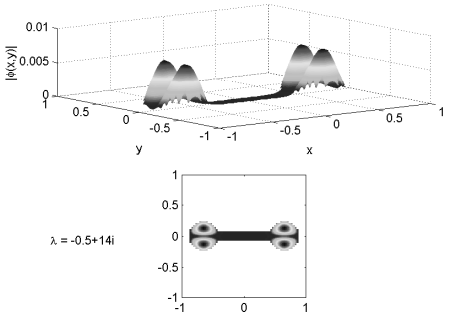

(a) Eigenfunction corresponding to strongly damped eigenvalue $\lambda = -0.5 + i\ 14$.

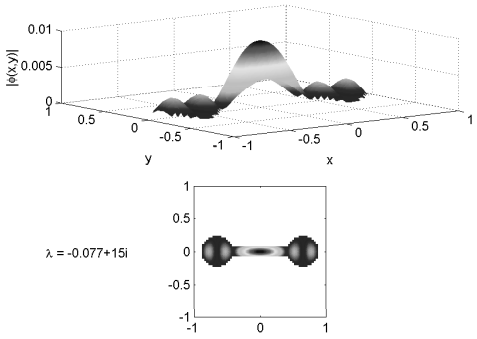

(b) Eigenfunction corresponding to lightly damped eigenvalue $\lambda = -0.077 + i\ 15$.

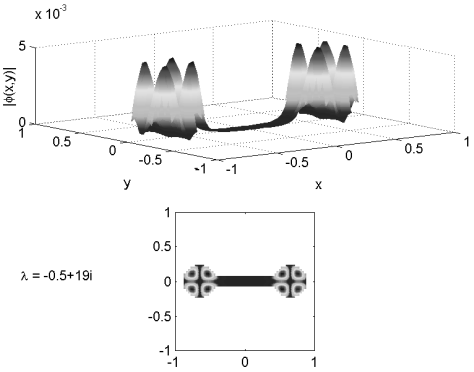

(c) Eigenfunction corresponding to strongly damped eigenvalue $\lambda = -0.5 + i\ 19$.

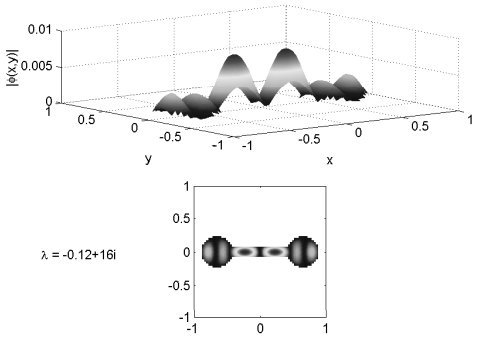

(d) Eigenfunction corresponding to light averagely damped eigenvalue $\lambda = -0.12 + i\ 16$.

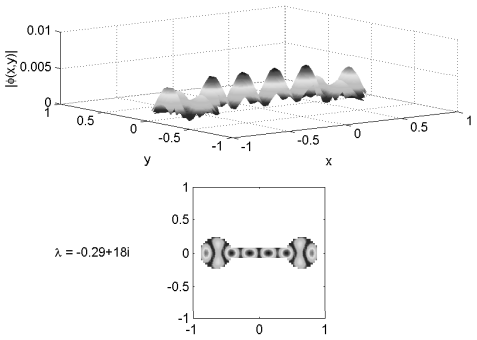

(e) Eigenfunction corresponding to averagely damped eigenvalue $\lambda = -0.29 + i\ 18$.

FIGURE 10. Eigenfunctions for damping on both discs of the dog-bone.

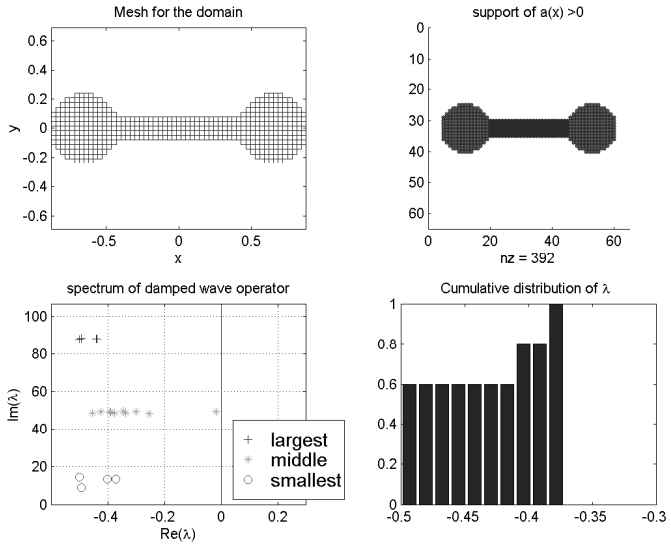

FIGURE 11. The dog-bone region with $a(x) = 1$ in both discs: mesh, damping, eigenvalues.

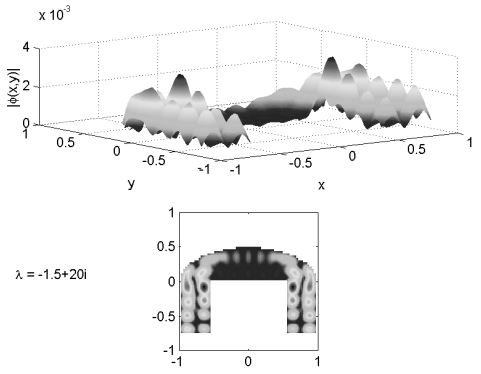

(a) Eigenfunction corresponding to strongly damped eigenvalue $\lambda = -1.5 + i\,20$.

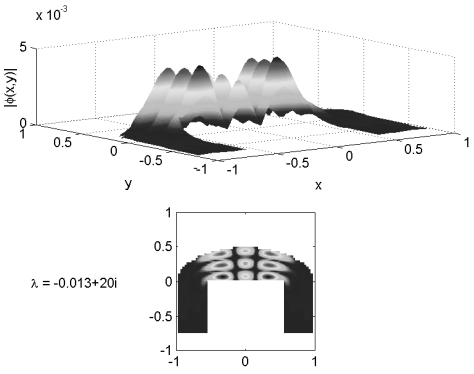

(b) Eigenfunction corresponding to lightly damped eigenvalue $\lambda = -0.013 + i\,20$.

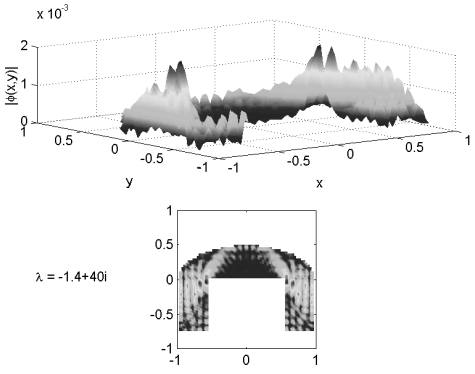

(c) Eigenfunction corresponding to strongly damped eigenvalue $\lambda = -1.4 + i\,40$.

FIGURE 12. Eigenfunctions for damping in both sleeves of the football jersey.

FIGURE 13. The football jersey geometry with $a(x) = 1$ in both sleeves (actual computations performed on the right-most case).

eigenvalues situated in the gap correspond to diffracted modes (exactly as one might expect from the physics.)

5. CONCLUSION

In conclusion, the numerical experiments have borne out our optimism concerning the strong links between the asymptotic distribution of the eigenvalues and the geometric damping. We have observed that "tracing the rays" of geometrical optics effectively leads to a very good appreciation of the eigenvalue distribution.

The MATLAB code used in this paper is freely available (as is) on the first author's web site at http://www.univ-tln.fr/~marka/damp. Full color graphics of all numerical results may also be found at this URL.

REFERENCES

[Cornfeld 82] I. Cornfeld, S. Fomin, and YA. G. Sinai. *Ergodic Theory.* New York: Springer-Verlag, 1982.

[Chen et al. 91] G. Chen, S. Fulling, F. Narcowich, and S. Sun. "Exponential Decay of Energy of Evolution Equations with Locally Distributed Damping." *SIAM J. Appl. Math.* 51:1 (1991), 206–301.

[Cox and Zuazua 94] S. Cox and E. Zuazua. "The Rate at which Energy Decays in a Damped String." *Comm. Partial Diff. Equations* 19 (1994), 213–243.

[Freitas 98] P. Freitas. "Optimizing the Rate of Decay of Solutions of the Wave Equation Using Genetic Algorithms: A Counterexample to the Constant Damping Conjecture." *SIAM J. Control Optim.* 37:2 (1998), 376–387.

[Freitas 99] P. Freitas. Private communication. 1999.

[Gérard and Leichtman 93] P. Gérard and E. Leichtnam. "Ergodic Properties of Eigenfunctions for the Dirichlet Problem." *Duke Math. Journal* 71:2 (1993), 559–607.

[Kuttler and Sillito 84] J. R. Kuttler and V. G. Sillito. "Eigenvalues of the Laplacian in Two Dimensions." *SIAM Review* 26:2 (1984), 163–193.

[Shubov et al. 97] M. Shubov, C. Martin, J. Dauer, and B. Belinskiy. "Exact Controllability of the Damped Wave Equation." *SIAM J. Control Optim.* 35:5 (1997), 1773–1789.

[Sjöstrand 00] J. Sjöstrand. "Asymptotic Distribution of Eigenfrequencies for Damped Wave Equations. *Publ. Res. Inst. Math. Sci.* 36:5 (2000), 573–611.

[Sorenson 95] D. C. Sorenson. *Implicitly Restarted Arnoldi/Lanczos Methods for Large Scale Eigenvalue Problems.* MATLAB documentation, 1995.

M. Asch, Laboratoire LAMFA, CNRS UMR 6140, Université de Picardie Jules Verne, 33 rue Saint Leu, 80039 Amiens Cedex 1, France (mark.asch@u-picardie.fr)

G. Lebeau, Laboratoire J. A. Dieudonné, UMR CNRS 6621, Université de Nice Sophia-Antipolis, 06108 Nice Cedex 2, France (lebeau@math.unice.fr)

Received June 11, 2002; accepted in revised form March 20, 2003.